



HAL
open science

Straining the root on and off triggers local calcium signaling

Vassanti Audemar, Yannick Guerringue, Joni Frederick, Pauline Vinet, Isaty Melogno, Avin Babataheri, Valérie Legué, Sebastien Thomine, Jean-Marie Frachisse

► **To cite this version:**

Vassanti Audemar, Yannick Guerringue, Joni Frederick, Pauline Vinet, Isaty Melogno, et al.. Straining the root on and off triggers local calcium signaling. 2026. <hal-04256220>

HAL Id: hal-04256220

<https://hal.science/hal-04256220v1>

Preprint submitted on 5 Mar 2026

HAL is a multi-disciplinary open access archive for the deposit and dissemination of scientific research documents, whether they are published or not. The documents may come from teaching and research institutions in France or abroad, or from public or private research centers.

L'archive ouverte pluridisciplinaire **HAL**, est destinée au dépôt et à la diffusion de documents scientifiques de niveau recherche, publiés ou non, émanant des établissements d'enseignement et de recherche français ou étrangers, des laboratoires publics ou privés.



Distributed under a Creative Commons CC BY-NC-ND 4.0 - Attribution - Non-commercial use - No Derivative Works - International License

1 **Straining the root on and off triggers local calcium signaling**

2

3 Vassanti Audemar, Yannick Guerringue, Joni Frederick, Isaty Melogno, Pauline Vinet, Avin
4 Babataheri, Valérie Legué, Sébastien Thomine*, Jean-Marie Frachisse*

5

6 Vassanti Audemar, Yannick Guerringue, Isaty Melogno, Pauline Vinet, Sébastien Thomine, Jean-Marie
7 Frachisse : Université Paris-Saclay, CEA, CNRS, Institute for Integrative Biology of the Cell (I2BC), 91198,
8 Gif-sur-Yvette, France.

9 Valérie Legué : Université Clermont Auvergne, INRAe, PIAF, F-63000 Clermont-Ferrand, France

10 Joni Frederick, Avin Babataheri : Laboratoire d'Hydrodynamique LadHyX, CNRS, École polytechnique,
11 Institut Polytechnique de Paris, 91120 Palaiseau, France

12 (*) S. Thomine and J-M Frachisse are Corresponding authors

13

14 **Classification:** Research Report, Plant Biology

15 **Keywords:** root, mechanotransduction, microfluidics, Arabidopsis, calcium signaling

16 **Highlights:**

17 - A microvalve concept mimicking lateral soil pressure was developed.

18 - Non-damaging lateral compression of the root induces an elastic deformation of cortical cells.

19 - A multicomponent calcium signal is elicited at the onset of a pressure pulse and upon release of the
20 pressure.

21 - Straining rather than stressing of tissues is relevant to trigger the calcium signal.

22 - The calcium signal is localized at the tissue under pressure and does not propagate.

23 - Calcium signals exhibit a remarkable attenuation upon repetitive stimulations.

24

25 **Abstract**

26 Throughout their life, plant roots are submitted to mechanical stresses due to pressure exerted by the
27 soil. So far, few studies addressed root cell deformation and calcium signaling elicited by soil
28 compression. In this study, we designed a microchip inspired by pneumatic microvalve concept in order
29 to deliver a lateral pressure to the root of a plant expressing the RGECO1-mTurquoise calcium reporter.
30 Lateral pressure applied on the root induced a moderate elastic deformation of root cortical cells and
31 elicited a multicomponent calcium signal at the onset of the pressure pulse, followed by a second one
32 at the release of the pressure. This indicates that straining rather than stressing of tissues is relevant
33 to trigger the calcium signal. The calcium elevation was restricted to the tissue under pressure and did
34 not propagate. Additionally, the calcium signals exhibited a remarkable attenuation upon repetitive
35 stimulations.

36

37 **Introduction**

38 Plants are anchored to the ground by their roots. They need to sense environmental cues to adapt to
39 external conditions. Among these cues are external forces like gravity, soil compression, wind or touch
40 by animals. In contrast to aerial organs, roots experience high mechanical stresses due to pressures
41 exerted by the soil. In order to penetrate the soil and to overcome physical obstacles, the root
42 generates an axial force. At the same time, during its progression, lateral confinement along the radial
43 axis increases, generating lateral forces [1], [2]. Soils scientists often consider “soil structure” as the
44 spatial arrangement of the different components and properties of soil [3]. A typical volume of surface
45 soil includes about 50% solids, mostly soil particles (45%), and organic matter (generally < 5%) and
46 about 50% pore space [1]. Therefore, during their growth, roots progress in a heterogeneous network
47 crossing empty cavities and substrates of various stiffness. The thrust force (or pushing force) exerted
48 by the growing part of the root has to overcome the soil resistance as well as the lateral friction with
49 the soil. The friction involved in the balance of forces is the one acting on the flanks of the root along
50 the elongation and meristematic zones [1]. A local lateral confinement around the radial axis is a
51 scenario that the root can encounter. Such a stress occurs for example upon radial growth of the root
52 squeezed between two hard fixed soil particles. To our knowledge, the characteristics of physical and
53 biological responses locally elicited by such a compressive, non-wounding stimulation, have so far not
54 been investigated.

55 Calcium is one of the most important ions for signal transduction. Free cytosolic calcium concentration
56 increases in response to many signals. The duration, amplitude, frequency and spatial distribution of
57 the calcium elevation is controlled by calcium channels, transporters and pumps localized at the cell
58 membranes [4]. The spatio-temporal pattern of cytosolic calcium elevation was shown to encode
59 information allowing specific responses to diverse cues that involve cytosolic calcium as a second
60 messenger [5], [6]. Notably, it has been shown that calcium is involved in signal transduction of touch
61 [7]. Rise and propagation of a calcium signal in the case of Venus flytrap induces the closing of the leaf
62 [8]. *Arabidopsis thaliana* also displays a calcium signal after local stimulation of a root cell with the tip
63 of a micropipette [7]. Macromolecules involved in the control of the wall integrity embedded in the
64 membrane or in the cell wall could be recruited for transduction of a mechanical stress into biological
65 responses including calcium variations [9]. For example, FERRONIA (FER), a transmembrane protein
66 was shown to be involved in root mechanoperception [10]. Moreover the *fer* mutant shows an
67 alteration of the calcium signal elicited by touching or bending the root [10]. The plasma membrane is
68 also subjected to mechanical stress due to tensile or compressive forces and variation of osmotic
69 pressure [11]. Calcium permeable mechanosensitive channels at the plasma membrane are good
70 candidates to mediate cytosolic calcium elevations in response to membrane deformation induced by
71 touch or cell compression. Thus far, five families of mechanosensitive channels MSL, Piezo, OSCA, MCA
72 and TPK have been molecularly identified and electrophysiologically characterized in *Arabidopsis* [12].
73 An additional mechanosensitive channel, non-molecularly identified, called RMA (Rapid Mechanically
74 Activated) from the plasma membrane of *Arabidopsis* was characterized [13]. All these
75 mechanosensitive channels except for MSL are calcium permeable but also permeable for other
76 divalent and monovalent cations. With rapid activation and inactivation, Osca, Piezo and RMA share
77 common kinetics properties [14].

78 Here we address the following questions: Could a compression mimicking the lateral confinement
79 generated by the soil pressure deform the root? What are the specific properties of the calcium signal
80 elicited by such strain? We developed a microfluidic device enabling us to apply a controlled
81 mechanical lateral stress on the root to address these questions. The microfluidic device allows
82 imaging of plant roots with a microscope for long durations with a high spatio-temporal resolution. We
83 used confocal microscopy to image and quantify cell deformation and Epifluorescence microscopy
84 combined with a fluorescent cytosolic calcium reporter to characterize the calcium signal induced by
85 lateral strain on *Arabidopsis thaliana* roots.

86

87 **Materials and Methods**

88 **Microfluidic device manufacturing**

89 The polydimethylsiloxane (PDMS) devices were made using standard dry film and soft lithographic
90 procedures based on the method by Dangla *et al.* (2013) [15]. To produce molds for the root growth
91 channels, two layers of Eternal Laminar E8020 dry photoresist film of thickness $49 \pm 2 \mu\text{m}$ were
92 successively deposited on a glass slide by lamination at 100°C to reach a desired channel height of
93 $\sim 100 \mu\text{m}$. The film was UV exposed through a photomask designed using CleWin5, to produce straight
94 channels with height, width and length of $\sim 90 \mu\text{m}$, $600 \mu\text{m}$ and 2 cm , respectively.

95 The channels were replicated from the master molds in degassed PDMS with a 1 to 10 ratio of curing
96 agent to bulk material (SYLGARD 184 elastomer and curing agent, Dow Corning), cured at 70°C for 2
97 hours to obtain the device pieces. PDMS blocks serving as root growth channels were replicated with
98 a strictly controlled height, so that once bonded to a glass coverslip, the top part of the channel leaves
99 a PDMS membrane with a thickness of 250 or $460 \mu\text{m}$ which serves as a deformable push-down valve.
100 PDMS blocks serving as pressure channels sitting above the plant growth channels were made using
101 the same procedure, and with a thickness of $4 \text{ mm} \pm 1 \text{ mm}$. A spin coater (Model WS-650MZ-23NPPB,
102 Laurell) was used to obtain a thin layer of PDMS to coat coverslips. Several devices with different
103 membrane thicknesses were produced by varying the time or rotational speed of the spin coating
104 process. Membrane thicknesses were measured by profilometry (ProFilm3D, Filmetrix)
105 (Supplementary Fig. 1). PDMS pieces were peeled off the molds, and pierced with 1 mm holes to create
106 liquid and gas inlets/outlets. Additional holes were punched at a 45° angle to serve as the entry path
107 connecting the root with the root growth channels before sealing by plasma treatment (Harrick
108 Plasma, Plasma Cleaner PDC-002-CE) together and to a glass coverslip covered with a thin (37 ± 2
109 μm) PDMS layer.

110 **Plant material and growth conditions.**

111 Seeds of *Arabidopsis thaliana* (Col-0 ecotype) constitutively expressing RGECO1-mTurquoise under the
112 UBQ10 promoter [16] were sterilized in ethanol 70% and SDS 0.05% for 5 min, rinsed with ethanol 96%
113 for 5 min and dried at room temperature. Then, the seeds were sown on conical cylinders produced
114 by cutting micropipette tips containing Hoagland medium ($1.5 \text{ mM Ca}(\text{NO}_2)_2$, $0.28 \text{ mM KH}_2\text{PO}_4$, 0.75
115 mM MgSO_4 , 1.25 mM KNO_3 , $0.5 \mu\text{M CuSO}_4$, $1 \mu\text{M ZnSO}_4$, $5 \mu\text{M MnSO}_4$, $25 \mu\text{M H}_3\text{BO}_3$, $0.1 \mu\text{M Na}_2\text{MoO}_4$,
116 $50 \mu\text{M KCl}$, 3 mM MES , $10 \mu\text{M Fe-HBED}$, pH 5.7) with 1% phyto-agar, they were inserted into the same
117 medium filling Petri dishes [17]. After 3 days of stratification at 4°C in the dark, the seeds were
118 incubated in 16h light/ 8h dark at 22°C during 3 days in a culture chamber. After the primary root
119 reached the bottom of the cone, they were transferred from the Petri dish to the microfluidic device
120 (Fig. 1b) and kept under the same temperature and light conditions. Root growth was conducted into
121 the root channel filled with liquid Hoagland. During the growth, the device was tilted with an angle $>$
122 45° to allow the root to grow gravitropically. Root channels were connected by tubing to syringes filled
123 with liquid Hoagland medium, and the channel medium was refreshed with a flow rate of $1 \mu\text{L}/\text{min}$
124 using a syringe pump.

125 **Acquisition protocol**

126 When root growth had extended passed the deformable membrane portion of the PDMS device, i.e.
127 6 or 7 days after transfer to the incubation chamber, microscopy experiments were launched. The root
128 channel was connected by tubing to syringes filled with liquid Hoagland medium and connected to a
129 syringe pump (WPI, AL-1000) enabling control of the flow rate. The pressure channels were connected
130 by tubing to a pressure box (Fluigent, MFCS-EX) that allows injection of an air flow at a fixed pressure
131 into these channels. The PDMS device was secured in a 3D printed sample holder fitted with a Perspex
132 lid and designed to fit in a standard 96-well plate sample holder.

133 Cross-sectional views of the microfluidic channels and cross sections of the roots were acquired with
134 a Leica SP8 inverted microscope equipped with, a white light laser (470 to 670 nm), and two GaAsP
135 Hybrid detectors (Hamamatsu). For cross sections of the channels, fluorescein solutions at 10 μ M were
136 imaged with a 10x PLAN APO dry objective (Leica) at λ_{exc} = 488 nm and λ_{em} = 501-609 nm. For cross
137 section of the roots, cell walls were labelled with propidium iodide (5 μ g/mL) and imaged using a 20x
138 PLAN APO multi-immersion objective (Leica), with λ_{exc} = 488 nm and λ_{em} = 551-651 nm. A Leica DMI
139 6000 inverted microscope equipped with an excitation lamp (PE-4000 LEDs, CoolLed), a quad band
140 dichroic mirror (Chroma) and black and white camera (CoolSNAP HQ² CCD, Photometrics) was used to
141 image intracellular calcium. RGECO1-mTurquoise fluorescent lines were imaged using a 5x dry
142 objective with λ_{exc} = 580 nm and λ_{em} = 600-700 nm for RGECO1 and λ_{exc} = 470 nm and λ_{em} = 490-
143 520 nm for mTurquoise.

144 **Image processing and data analysis**

145 Image processing and analysis was performed using Matlab. Length variations of cells along Oy and Oz
146 axis (Fig. 3) were measured on cross-sectional views of wild type roots stained with propidium iodide.
147 Image analysis was conducted following these steps : the background was subtracted and a
148 segmentation was performed to delimit cell boundaries. Maximal length of each cell in the horizontal
149 and vertical dimension was measured before and during the pressure stimulation using bounding box
150 (Supplementary Fig. 2). Calcium signal variation measurements were performed as follows : for each
151 time point, the background was subtracted and a binary image was generated. The root axis was
152 extracted and segments of 100 μ m perpendicular and centered around this axis were distributed at 50
153 pixels intervals (Supplementary Fig. 2d). Mean values of the ratio between RGECO1 images and
154 mTurquoise images were calculated for each segment along the root and reported in heat maps
155 representing calcium signal variations along the root axis over time.

156

157 **Results**

158 **Setting up a micromechanical system for delivering lateral pressure**

159 In order to apply a controlled lateral compression to the root, we have developed a microfluidic device
160 combining a rootchip [17] with a pressure system inspired by a micromechanical push-up valve [18].
161 The device was fabricated in PDMS which has been shown to be biocompatible with *Arabidopsis*
162 *thaliana* [19]. Three layers of PDMS were sealed together, enabling the formation of channels: the
163 pressure channels containing air sit on top of the root channels in which the root is growing, while the
164 whole PDMS device is bound to a glass coverslip covered in a thin PDMS film to enable the visualization
165 of the root with an inverted microscope (Fig. 1a).

166

167 The perpendicular layering of the root channel and pressure channels defines a square PDMS
168 membrane (Fig. 1b) with an active area of 600 μ m by 600 μ m (Fig. 1c). The PDMS deformability and
169 the specific dimensions, especially the thickness/side length aspect ratio, allow the membrane to
170 deflect downward into the root channel when a sufficiently high pressure is injected into the pressure
171 channel. In our device, two of these micromechanical push-down valves are distributed 2 mm apart
172 over the root channel (Fig. 1b), and each pressure channel can be controlled individually.

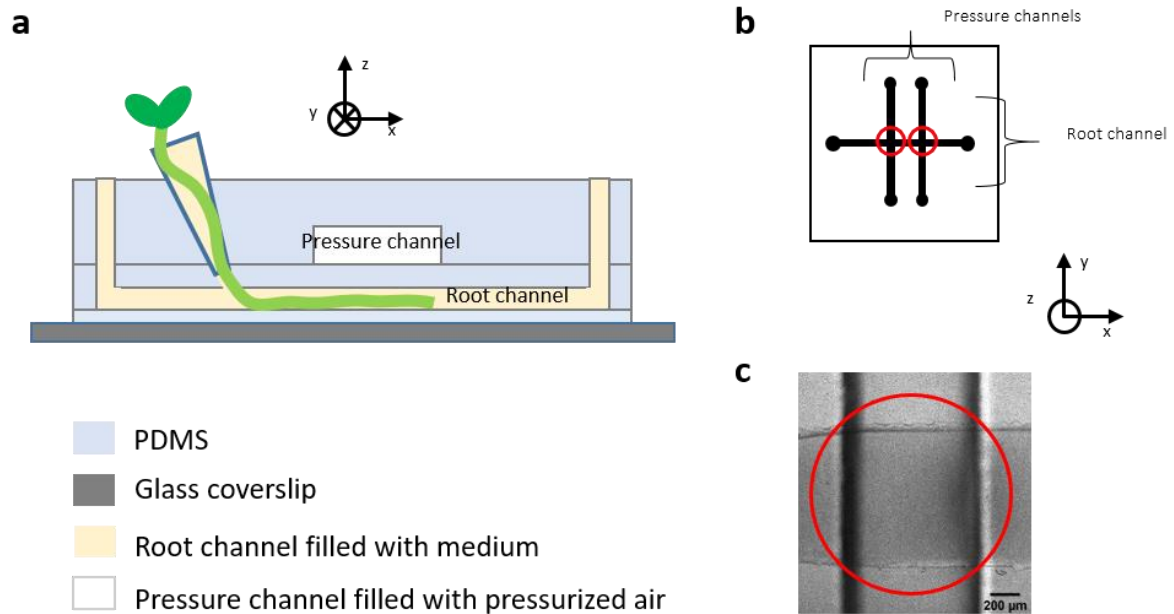
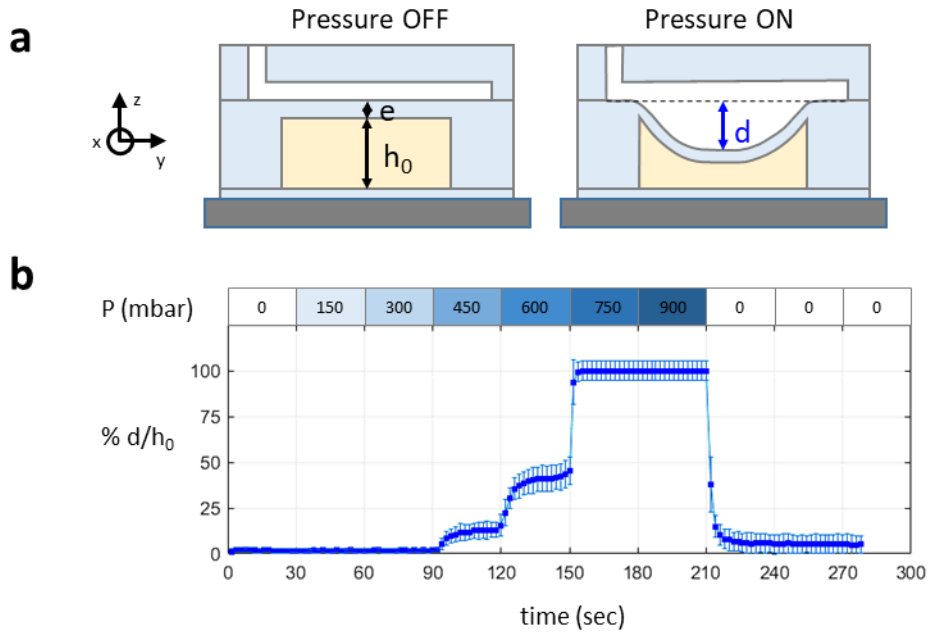


Figure 1: Microfluidic device equipped with a pneumatic valve. a) Schematic side view of the microfluidic device containing the plant root channel and pressure channel separated by a flexible push-down PDMS valve. b) Schematic top view of the 2 mechanical push-down valves at the intersections of the root channel and the pressure channels. c) Top view of a mechanical push-down valve imaged in bright field (Leica DMI 6000, 5x objective). In 1.c and 1.d, valves areas have been circled in red.

We compared the deflection, d , of the push-down membrane of microfluidic devices with 2 different membrane thicknesses: $460 \pm 57 \mu\text{m}$ and $250 \pm 31 \mu\text{m}$ (as annotated in figure 2a). The $250 \mu\text{m}$ PDMS membrane exhibits a greater deformability for the same pressure (shown in cross-sectional views of the root channels without root perfused with a solution of fluorescein at $10 \mu\text{M}$ with a constant flow rate of $8 \mu\text{L}/\text{min}$; [supplementary Fig. 3](#)). A compromise had to be made for the PDMS membrane thickness to be thin enough to increase the deformability and enable a good transfer of pressure from the pressure channel to the root, but thick enough to avoid damage during the device manufacturing process. In further experiments, the PDMS membrane thickness was fixed at $250 \mu\text{m}$.



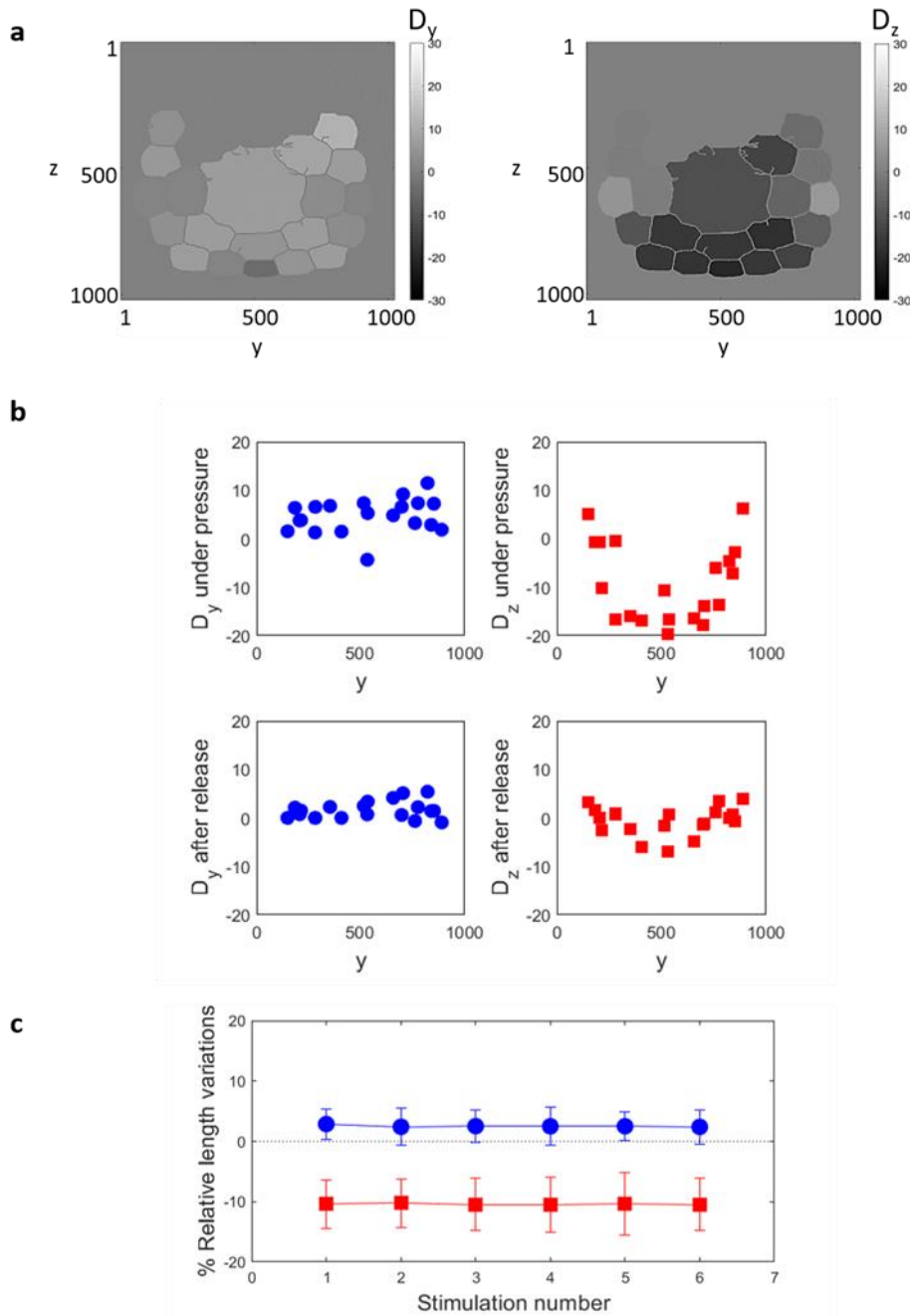
187 **Figure 2:** Relationship between membrane deformation and pressure in the air channel. a) Schematic cross
188 section of the pneumatic valve with and without pressure: e is the thickness of the PDMS membrane separating
189 the pressure channel (white) and the root channel (yellow), h_0 is the height of the root channel before pressure
190 and is equal to $90\ \mu\text{m}$, d is the maximum distance between the center of the valve membrane at rest and in its
191 deformed state when pressure is applied. b) Variations of d , the maximal deformation of a $250\ \mu\text{m}$ thick PDMS
192 membrane with applied pressure. Measurements were repeated 3 times on 4 different valves. Squares
193 correspond to the mean values of all measurements and error bars correspond to standard deviations.

194 We measured the deflection of the $250\ \mu\text{m}$ PDMS membrane as a function of the pressure increasing
195 by steps of 150 mbar every 30 seconds. The percentage of the deflection length, d , normalized by the
196 thickness of the channel h_0 is presented in figure 2b. Deformation is triggered with pressure from 450
197 mPa and continuously increases with pressure, until the valve membrane reaches the bottom of the
198 channel ($d = h_0$) at 750 mPa. This system without root has a typical time to reach the equilibrium state
199 of around 10s. Upon release of the pressure, the membrane returns to its approximate initial position.
200 The number of stimulations on the same valve does not impact its ability to deform. The short standard
201 deviation bars indicate that the system is reliable and does not experience damage with repeated
202 stimulations.

203

204 Lateral pressure induces quasi-elastic deformation of the root cells

205 We assessed the mechanical response to a pressure of 900 mbar applied through the deformable
206 PDMS membrane (also called valve) on primary roots of 7 days old seedlings in the maturation zone
207 (1-5 mm from the apex). Confocal images of root cross sections were used to measure the deformation
208 of the root in the Oyz dimension. Cell walls were stained with propidium iodide to visualize cell shape.
209 A segmentation analysis was performed to identify the outlines of cells ([Supplementary figure 1a](#),
210 [Supplementary video 1](#)). We measured the length of the cells, L_y and L_z projected on the Oy and Oz
211 axes, transversal and longitudinal to the applied force respectively. D_y and D_z are the corresponding
212 relative length variations defined by $D_y = (L_y - L_{y0})/L_{y0}$ and $D_z = (L_z - L_{z0})/L_{z0}$, with L_{y0} and L_{z0} the projected
213 length on Oy and Oz axes before the application of the pressure. Cells located in the upper part of the
214 image were out of the working distance of the objective and therefore could not be segmented. Cell
215 walls located in the central cylinder were not stained by propidium iodide and therefore were not
216 segmented, thus we consider the central cylinder as one object.



217

218 **Figure 3:** Transversal and longitudinal relative length variations D_y and D_z : a) Representation of the segmented
 219 cells of one representative root under a pressure stimulation of 900 mbar. Each cell was colored with a grey level
 220 corresponding to the percentages D_y on the left and D_z on the right. b) Percentage D_y and D_z of one representative
 221 root during the first stimulation and after the release in function of the transversal dimension O_y . c) Percentages
 222 D_y and D_z averaged over all the segmented cells of a root stimulated 6 times every 5 min with a pressure of 900
 223 mbar during 1 min. The plain symbols represent the mean value of 19 different roots and the error bars represent
 224 the standard deviation associated. For b) and c), the blue circles and red squares correspond to D_y and D_z
 225 respectively.

226 Under pressure, D_y and D_z show a heterogeneous repartition between the cells of the cross-section
 227 due to the geometry of the applied force and the connectivity between the cells (figure 3a), resulting
 228 in a complex tension field. For example, the cells located on the lateral sides experience a positive
 229 variation length D_z , indicating an elongation instead of the compression observed among the other
 230 cells. Figure 3b shows the repartition of D_y and D_z along the transversal axis O_y for the root under
 231 pressure and after release. The distribution of D_y is roughly constant along the O_y direction whereas

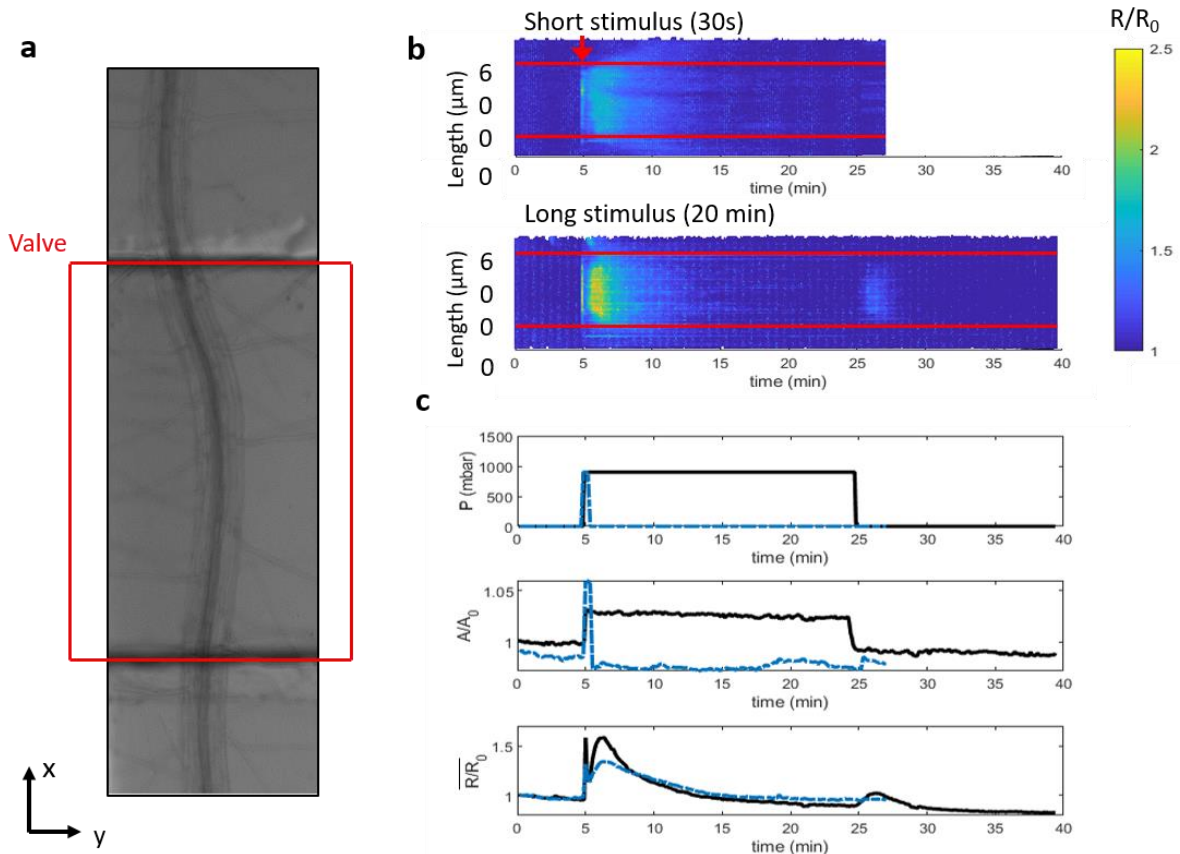
232 Dz experiences a symmetrical distribution with respect to the midline of the root in the Oz direction,
233 with the largest relative length variations corresponding to the cells close to the midline (fig. 3a). After
234 release of the pressure, the initial cell shapes were recovered with values of D_y and D_z close to 0 %,
235 showing a quasi-reversible deformation process.

236 Six repeated stimulations every 5 minutes have been performed on roots with a pressure of 900 mbar
237 during 60 seconds, on 19 roots in the maturation zone (1-5 mm from the apex). The average
238 percentages of D_y and D_z over all the cells per root were calculated. No correlation was revealed
239 between the average percentage of length variations and the position along the main axis. Under a
240 stimulus of 900 mbar, D_z was around 10 % and D_y around 4%. After 6 stimulations, no significant
241 differences in relative length variation was found as shown in figure 3c.

242

243 **Mechanical stimulus elicits a local elevation of cytosolic calcium concentration**

244 We used the fluorescent ratiometric reporter RGECO1-mTurquoise [16] to monitor cytosolic calcium
245 variations in roots. The reporter was constitutively expressed into the cytosol of plant cells, and we
246 measured the ratio R between the RGECO1 fluorescent signal, sensitive to the calcium concentration,
247 and the mTurquoise fluorescent signal, used as a control of the expression of the reporter. The
248 normalized ratio R / R_0 , with R_0 corresponding to the baseline value of R before any stimulation, was
249 represented by heat maps in Fig. 4b, as a function of the time and the position along the main root axis
250 for two types of stimulation at 900 mbar: a short stimulation of 30 s, or a long stimulation of 20 min.
251 In either case, we observed a calcium signal rapidly increasing and progressively decreasing back to
252 the basal level approximately 15 min after the beginning of the stimulation ([Supplementary video 2](#)).
253 In the case of the long stimulation, a second increase of calcium signal is elicited by the release of
254 pressure. On a spatial level, the calcium signal mainly stays between the boundaries of the valve and
255 no clear propagation along the root axis was noticed. The normalized projected area A / A_0 and the
256 average value of the ratio $\overline{R} / \overline{R}_0$ were calculated on the portion of the root located under the valve
257 and are represented in Figure 4c with the pressure protocol associated. In either case, the variation of
258 the projected area was around 5% and recovered its initial level after the release of pressure, indicating
259 a small elastic deformation. The average value of the ratio $\overline{R} / \overline{R}_0$ displays a multicomponent signal
260 with two distinguishable phases: a rapid and sharp elevation with a maximum occurring at 10 ± 3.7 s
261 after the beginning of the stimulation, followed by a smoother rise and decrease of the signal with a
262 maximum a 100 ± 15.5 s, that ends up recovering its initial value within 15 minutes.

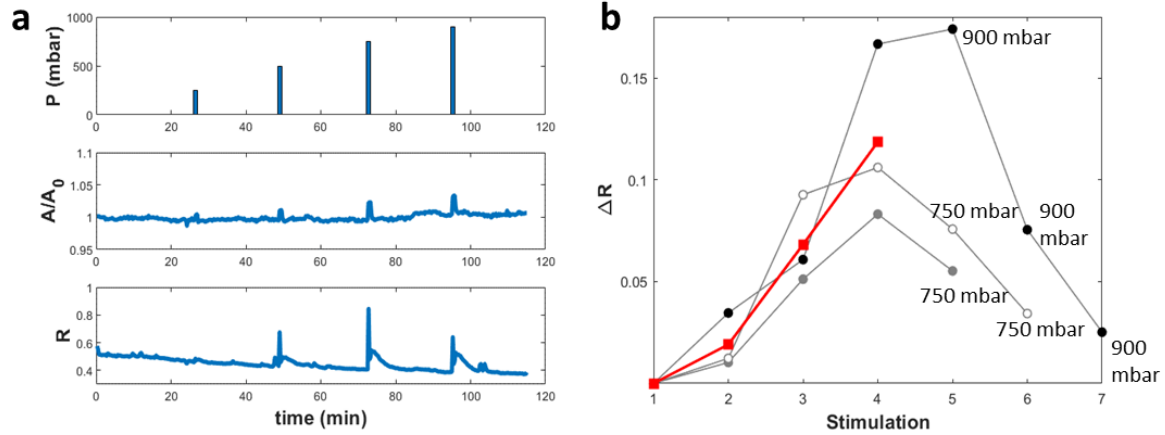


263
264 **Figure 4:** Calcium response, in time and space, to a local short (30 s) and long (20 min) applied pressure of 900
265 mbar: a) Bright field image of the root under the pneumatic valve. b) Variations of the normalized ratio R/R_0
266 along the main root axis x during time, represented as heat maps for a 30 s stimulus (top image) and a 20 min
267 stimulus (bottom image). The red lines correspond to the position of the pneumatic valve and the red arrows to
268 the time of stimulation (activation and release). c) Time variations of the pressure stimulation (top), the
269 normalized projected area of the root (middle) and the calcium signal ratio normalized to the value at time 0
270 (bottom) elicited by a pressure of 900 mbar during 30s (dotted blue line) and 20 min (black line). The graphs
271 show one representative experiment out of 23 for short and 10 for long stimulation.

272

273 **The amplitude of the cytosolic calcium signal increases with increasing pressure intensity**

274 In order to analyse the relationship between the pressure intensity and the amplitude of the cytosolic
275 calcium signal, we subjected the root to mechanical stimulations of 30 s with an increasing pressure
276 intensity using the pressure protocol presented in Figure 5a (top panel). The normalized area
277 presented in Figure 5a (middle panel) show an increase corresponding to the increasing pressure. We
278 can also observe the increase of the amplitude of the calcium signal as represented in the figure 5b.
279 Note that the amplitude of the initial fast increase was not measured because the acquisition rate in
280 this experiment was not sufficient to resolve it. However, repetition of the pressure stimulation at 750
281 mbar (for 2 plants) or further increase to 900 mbar (1 plant, Fig. 5) triggered a rise in cytosolic calcium
282 with a lower amplitude. This indicates that the system is indeed sensitive to the intensity of pressure
283 and suggests that it undergoes attenuation upon repetitive stimulations.

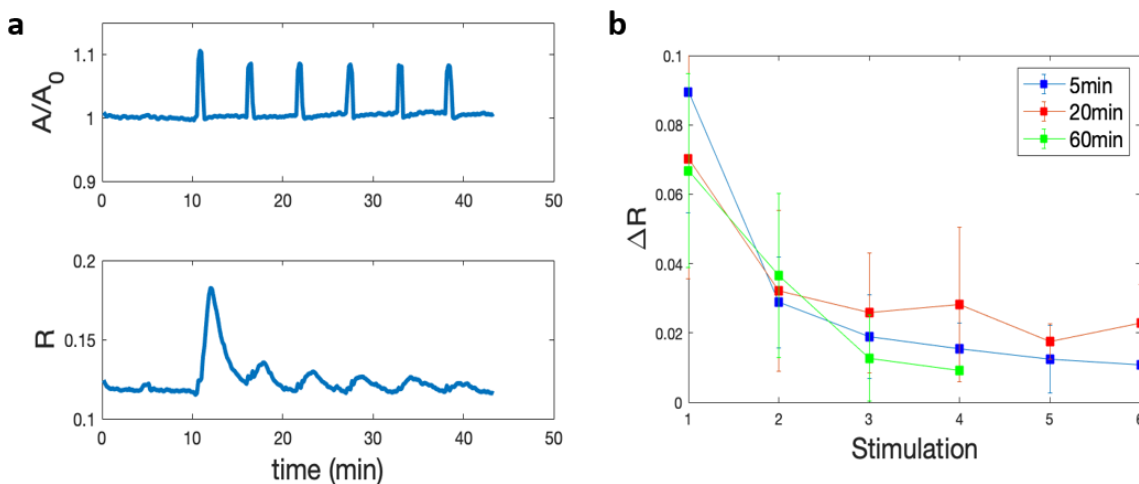


284

285 **Figure 5:** Successive stimulations of 30 s with an increasing pressure: a) pressure (top), normalized area (middle)
286 and calcium signal ratio (bottom) for one representative plant. b) Amplitude of the calcium signal for each
287 stimulation in three different roots represented in black, grey and white disks. Stimulations 2, 3 and 4 correspond
288 to 250, 500, and 750 mbar, respectively. Stimulations 5 to 7: pressure as indicated on the graph. The red squares
289 correspond to the mean value for the first 3 stimulations at 250, 500 and 750 mbar.

290 Repeated stimulations lead to attenuation of the calcium signal

291 To test whether the decrease of the calcium signal upon increasing pressure stimulation (Fig. 5) is due
292 to an intrinsic attenuation, we tested the effect of repetitive stimulations of the same amplitude. In
293 Figure 6, we subjected roots to repetitive pressure stimulations of 30 s at 900 mbar every 5 min. The
294 calcium signal in response to the first pressure pulse presented the highest intensity. The amplitude of
295 the second peak was decreased by more than 50% compared to the first one, while the amplitude of
296 following peaks subsequently decreased following each stimulation. These results indicate that the
297 system displays attenuation upon repeated stimulation. To test the effect of the frequency of
298 stimulation, and whether the system recovers from habituation after a longer delay, we imposed 30
299 second stimulations at different time intervals. In Figure 6C, the time interval between two pulses was
300 increased to 20 min or 60 min. The amplitude of the calcium rise decreased irrespective of the delay
301 between two stimulations. This indicates that the relevant factor for habituation is the number of
302 stimulations rather than their frequency, and that the calcium dynamics system does not recover after
303 60 min.



304

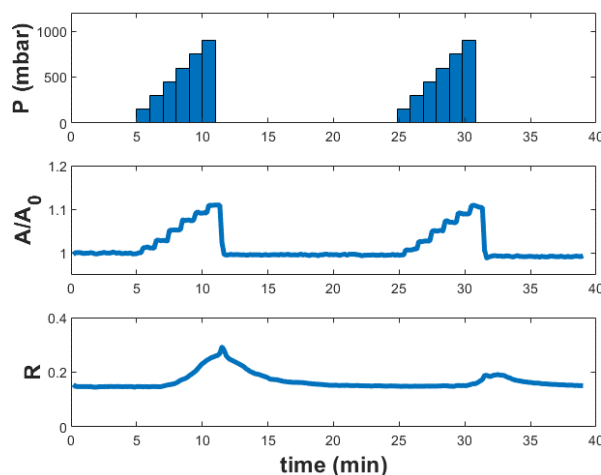
305 **Figure 6:** Repeated pressure stimulations lead to a decrease in the amplitude of the calcium signal. a) normalized
306 area variations (top) and calcium signal ratio (bottom) in a representative experiment, b) mean value of

307 maximum amplitude (+/- SD) of the calcium ratio peaks for each stimulation of 30 s at 900 mbar every 5 min (blue,
308 n = 6), 20 min (red, n = 5) and 60 min (green n = 4).

309

310 **A progressive rise of pressure drives a different calcium signature**

311 To apply a pressure stimulation that may correspond better to the stimulation experienced by a root
312 growing between hard obstacles, we applied a progressive increase of pressure by steps of 150 mbar
313 from 0 to 900 mbar every 60 seconds (Fig. 7). This stepwise increase was followed by a fast release of
314 pressure. We repeated this protocol two times on the same portion of the root with a time interval of
315 20 min. In this configuration, the area deformation shows a stepwise increase and decrease after
316 release of pressure corresponding exactly to the stepwise variations of pressure. A total recovery of
317 deformation was observed after release of the pressure. The second stepwise stimulation gave rise to
318 the same deformation. Compared to a one step increase, the calcium signal displayed a totally different
319 shape with of slow integrated increase and no decomposition in two phases, and a lower amplitude.
320 This shape could be due to an overlap between the rise and the decrease of the calcium signals
321 triggered at each step. When the pressure was released from 900 mbar to 0 in a short time scale, a
322 rapid increase was observed followed by a slow decrease to reach the baseline about 20 min later.
323 Upon the second stepwise stimulation, the calcium increase appeared only at the highest pressure and
324 its amplitude was reduced. This suggests that the calcium signal attenuation is associated with a
325 decreased sensitivity to pressure.



326 **Figure 7:** Calcium response to stepwise increases in lateral compression of the root. (top) Pressure increasing
327 by steps of 150 mbar from 0 to 900 mbar every 60 seconds followed by release to 0 mbar. This stimulation was
328 performed 2 times with a 20 min interval on a single root, (middle) Area variations with pressure stimulation
329 over time, (bottom) calcium signal ratio over time.

331

332 **Discussion**

333 We designed a microfluidic device allowing reproducible mechanical stimulations of roots. Our
334 experimental design proved to be suitable for investigating root deformation together with calcium
335 variation induced by a mechanical constraint. Precise description of the strain at tissue and cellular
336 levels, generated by a local compression was achieved. The analysis of the cytosolic calcium
337 concentration, in terms of kinetics, intensity and tissue location allowed us to characterize the Ca^{2+}
338 signal and to link it with the local strain.

339 This system could be used to monitor a wide range of cellular parameters and events in response to
340 gentle pressure stimulation. For example, the characterization of organelle shape and position upon
341 mechanical stress would bring valuable information. Considering the variety of fluorescent probes now
342 available and the ability to label proteins involved in mechanosensing, our system should allow
343 addressing key questions in mechanotransduction such as, for example, microtubule reorganization
344 and membrane tension variation.

345 *The calcium signature in response to mechanical stress*

346 We observed a calcium signal composed of two components, a fast calcium increase peaking after a
347 few seconds and a slower calcium response lasting a few minutes (Fig. 5 and 7), which are not
348 propagated along the root. Monshausen et al. [7] also showed that both touching the surface of the
349 Arabidopsis root or bending the root elicited a local calcium elevation. In both cases, the cytosolic
350 calcium concentration rapidly increased and then returned to its initial concentration 10 minutes after
351 bending and 60 seconds after touching. Mousavi et al. [20] monitored the calcium response to non-
352 damaging mechanical indentation of the root cap of Arabidopsis. Likewise, increasing the amplitude of
353 the indentations elicited a transient and localized Ca^{2+} signal in the columella and lateral root-cap cells.
354 In addition, they showed that depleting the plant from the mechanosensitive channel PIEZO1
355 diminished the calcium transient [20]. When bending Arabidopsis root, Shih et al. [10] elicited a
356 biphasic calcium response composed of a short peak followed by a longer wave. The longer wave was
357 attributed to the activation of the Receptor-like Kinase FERONIA. A biphasic calcium response was also
358 elicited by ATP in Arabidopsis roots. Matthus et al. [21] attributed the slow component to the
359 activation of the plasma membrane receptor DORN1/P2K1, while the rapid component was attributed
360 to the mechanical perturbation of the root through the experimental system. The calcium signature
361 elicited by gentle mechanical stimulation is distinct from the signal induced by salt stress or wounding.
362 Local treatment of the root with NaCl triggers Ca^{2+} waves that propagate through the plant at rates of
363 up to $\sim 400 \mu\text{m/s}$ [22]. Calcium signaling induced by wounding the aerial parts or the root elicited a
364 propagated wave of calcium delivering an information to remote organs [23].

365 Compared to previous studies, our microfluidic set-up revealed new features of the calcium response:
366 (i) a calcium elevation is observed upon increase but also upon release of the pressure, (ii) the intensity
367 of the calcium response increases with the pressure applied and (iii) Successive pressure stimuli lead
368 to attenuation of the calcium signal.

369 *Attenuation*

370 We have shown two important properties of the calcium signal, (1) after a rapid raise of calcium the
371 signal slowly recovers its initial level after 10 minutes whether the pressure is sustained or not, and (2)
372 the repetition of stimulations leads to a decrease in the amplitude of the calcium signal. Rapid increase
373 in calcium, in response to various physical stimuli such as cold shock, osmotic shock or touch has been
374 reported in plants [7], [24], [25]. These three stimuli, when sustained, the calcium concentration
375 rapidly decreases within a few tens of seconds to a few minutes after the initial peak. In Arabidopsis
376 and tobacco plantlets, the cold-induced increase in calcium is attributed to an influx of Ca^{2+} from the
377 extracellular medium relayed by an intracellular store. Then, recovery would be due to ER and vacuolar
378 uptake of calcium from the cytosol [24]. In Arabidopsis guard cells, performing successive depolarizing
379 hyperosmotic KCl shocks, the authors showed that cytosolic Ca^{2+} concentration controls stomatal
380 closure by two mechanisms, a short term 'calcium-reactive' closure and a long-term 'calcium
381 programmed' steady-state closure [25]. Furthermore, similar to our results, an attenuation of the
382 calcium signal is noticed upon repetition of the 5 minute KCl shocks every 10 minutes.

383 As part of an integrative approach, Martin et al. [26] have addressed the effect of wind stress on plant
384 growth and gene activation by performing multiple stem bending on young poplars. They observed a
385 decrease of the molecular response to subsequent bending as soon as a second bending was applied.
386 They called this phenomenon desensitization and determined a refractory period of 7 days needed to
387 recover a gene expression activation similar to that observed after a single bending.

388 The processes of amplification, attenuation and desensitization of the electrical signal have been the
389 most investigated in the neural system in the context of the transmission of information. In neurons,
390 the action potential (AP) might fire up to a frequency of 500 Hz. In this system, the transmission of
391 signals via chemical synapses represents a very dynamic process. The synapse, playing a role of relay,
392 is able in situations of prolonged stimulation to attenuate the signal [27]. The purpose of such an
393 attenuation would be to process the information and to adapt to an excess of signal, such as mentioned
394 for the auditory system [28]. The shape and the amplitude of the signal can be directly modified by the
395 ion channels generating the AP. For example, in the case of a high stimulation frequency, some
396 channels still being in their relative refractory period, APs will be modified in their shape and/or their
397 frequency [29]. It is also exemplified by Cain et al. [30] who showed that the kinetic properties of
398 several isoforms of T-type calcium channels are closely linked to their contribution to neuronal firing.
399 Mutations of T-type calcium channels would be associated with certain pathophysiological disorders.
400 The examples of attenuation mentioned above operate at different time scales, from milliseconds for
401 APs in a nerve, to minutes in guard cells and roots of Arabidopsis, and up to days for poplar gene
402 expression. Nevertheless, in all examples mentioned, attenuation leads to an adaptive response of the
403 cell/organ/organism, and the primary actors of the generation of the signal are likely ion channels.

404

405 *Strain-stretch hypothesis, its physiological relevance*

406 Calcium release is triggered at the onset of pressure and at the release of the pulse of pressure.
407 Similarly, responses to “touch” and “letting go” have been reported for epidermis cells of Arabidopsis
408 and tobacco [31]. In that case, distinct characteristics of the waves elicited by the compressive force
409 and its release suggest different underlying mechanisms for the “touch” and “letting go». In our
410 experiments, calcium release corresponds to the time when the maximum of strain variation in the
411 root cells is observed. Indeed, tissue shape variation occurs when strain is applied and released.
412 Although they differ in amplitude, probably due to attenuation, the calcium waves elicited by pressure
413 and release share the same characteristics. This indicates that strain rather than stress triggers calcium
414 signals underpinned by a common mechanism.

415 In biological materials, stress is not proportional to strain, therefore stress-sensing and strain-sensing
416 mechanisms have different output [32]. For example, in Arabidopsis pavement cells, microtubules,
417 which align in the direction of maximal mechanical stress, are postulated to play a role as a
418 mechanosensor [33]. However, James et al. reported that more generally the stimulus for growth
419 sensed by cells is the mechanical strain rather than the stress [34]. Furthermore, in agreement with
420 our finding, Moulia et al. showed that the strain-sensing model is better suited than the stress-sensing
421 model to explain the primary and secondary thigmomorphogenic growth-responses in trees [35].

422 Several recent studies highlight the role of calcium in long distance systemic signaling. Calcium
423 signaling induced by wounding aerial part or root elicited a propagating wave of calcium delivering
424 information to remote organs [23]. Here, with gentle local pressure the signal is restricted to the
425 pressurized zone. Only strained tissues display a calcium signal. This signaling path probably indicates
426 that cells have to react and adapt to the local deformation of the root. Thus, when a root is squeezed

427 between hard objects such as stones, lateral tissues are likely pressure-stimulated, inducing a local
428 calcium signal allowing the plant to adapt to this local soil constraint.

429 *What could be the molecular mechanisms underlying the calcium increase?*

430 Although the calcium signature in response to mechanical cues displays common features, the
431 molecular players remain elusive. Not only are the number of candidate receptors and channels
432 possibly involved in Ca^{2+} response numerous, but also calcium sources are diverse. Indeed, many Ca^{2+}
433 reservoirs are present in the cell, notably the vacuole, the endoplasmic reticulum (ER) and other
434 organelles [36], [37]. The kinetic behavior of transient Ca^{2+} signals was modeled at the cell level and
435 proposed to result from four components, two Ca^{2+} permeable channels located at the plasma- and
436 endo-membrane, respectively, and two active Ca^{2+} efflux systems, a Plasma membrane -based Ca^{2+}
437 ATPase pump and endomembrane-based $\text{Ca}^{2+}/\text{H}^{+}$ exchanger [4]. In our case, one can hypothesize that
438 the short peak relies on the activation of mechanosensitive channels, which immediately activate upon
439 membrane tension. The slower Ca^{2+} variation might recruit internal stores of calcium (ER, vacuole, ...)
440 governed by receptors involved in mechanosensing, such as FERONIA or DORN1.

441 At the cell membrane scale, Ca^{2+} permeable channels activated by a force applied in the plane of the
442 membrane were recently identified and characterized. These channels, such as RMA-DEK dependent
443 channels or those belonging to Oosca and Piezo families, behave as transducers able to convert
444 instantaneously a mechanical force into a Ca^{2+} flux [13], [20], [38]. One might hypothesize that a
445 pressure locally exerted on the root induces tissue strain that leads to membrane stretching. In
446 reaction to membrane stretching, calcium permeable mechanosensitive channels will be activated.
447 Most of these channels (RMA, Oosca, Piezo) present inactivation properties, meaning that a rise of
448 pressure applied to the membrane activates the channel, but under sustained pressure the channel
449 enters a non-conductive state called inactivated [14]. This inactivation might, at least in part, explain
450 the rapid (1-2 min) decrease of the Ca^{2+} signal under a long pulse of pressure delivered by the valve. In
451 our proposed scheme, the decrease of effective response to repetitive stimulation, that we call
452 attenuation, would be provided by a mechanical modification of cellular structural elements. An
453 increase in the cell stiffness would limit membrane stretching and then produce less activation of
454 calcium permeable mechanosensitive channels. Whether the cytosolic Ca^{2+} elevation plays a role in
455 this feedback loop remains to be investigated. Even though Ca^{2+} permeable force gated channels
456 appear to be the best candidates to mediate the coupling between mechanical strain and cytosolic
457 Ca^{2+} increase, other sensors of mechanical strains may also be involved, for example, the cytoskeleton
458 itself, or sensors of cell wall integrity [9], [39], [40].

459

460 *What could be the adaptive outcome of local calcium signaling?*

461 A root growing in the soil squeezed between two rocks, for example, will have to locally adapt its
462 mechanical properties by strengthening its tissues. This could be achieved through strengthening the
463 cell wall or remodeling the cytoskeleton. The non-propagated Ca^{2+} signal locally initiated by pressure
464 stimulation (mimicked in the experiment represented in Figure 7) might be the event that initiates
465 further transduction signaling cascades possibly involving pH variation, reactive oxygen species
466 emission, and kinase activation, and further leading to developmental responses and to the root
467 adaptation [5], [6]. In natural conditions, roots are also subjected to diurnal hydraulic pressure
468 variations producing a periodic root diameter increase and decrease ([41]). This latter phenomenon
469 has to be considered together with root progression in which a root squeezed in a bottleneck will be
470 self-stimulated during growth. Root curvature additionally induces strains, and secondary roots

471 preferentially emerge in the curved zones of the root [42]. This could be another adaptive response
472 triggered by pressure stimulation of the root.

473

474 **Acknowledgements**

475 Seeds expressing R-GECO were provided by Rainer Waadt and Melanie Krebs (Ruprecht-Karls-
476 Universität Heidelberg, Germany). This work has benefited from a French State grant (Saclay Plant
477 Sciences, reference n° ANR-17-EUR-0007, EUR SPS-GSR) under a France 2030 program (reference n°
478 ANR-11-IDEX-0003) through the DYNANO project. It has also benefited from Imagerie-Gif core facility
479 supported by l'Agence Nationale de la Recherche (ANR-11-EQPX-0029/Morphoscope, ANR-10-INBS-
480 04/FranceBioImaging ; ANR-11-IDEX-0003-02/ Saclay Plant Sciences). We gratefully acknowledge the
481 financial support from the Région Ile de France through the DIM ELICIT program, for the Plantuidics
482 grant. We thank David Bouchez from IJPB (Versailles, France) for fruitful discussions and Nicolas
483 Valentin for printing adapters to set up microfluidic chips of the microscopes.

484

485

486 **Bibliography**

- 487 [1] E. Kolb, V. Legué, et M.-B. Bogeat-Triboulot, « Physical root–soil interactions », *Physical Biology*,
488 vol. 14, n° 6, p. 065004, nov. 2017, doi: 10.1088/1478-3975/aa90dd.
- 489 [2] J. Roué *et al.*, « Root cap size and shape influence responses to the physical strength of the
490 growth medium in *Arabidopsis thaliana* primary roots », *Journal of Experimental Botany*, p.
491 erz418, nov. 2019, doi: 10.1093/jxb/erz418.
- 492 [3] A. R. Dexter, « Advances in characterization of soil structure », *Soil and Tillage Research*, vol. 11,
493 n° 3-4, p. 199-238, juin 1988, doi: 10.1016/0167-1987(88)90002-5.
- 494 [4] J. Bose, I. I. Pottosin, S. S. Shabala, M. G. Palmgren, et S. Shabala, « Calcium Efflux Systems in
495 Stress Signaling and Adaptation in Plants », *Front. Plant Sci.*, vol. 2, 2011, doi:
496 10.3389/fpls.2011.00085.
- 497 [5] B. Ranty, D. Aldon, V. Cotelle, J.-P. Galaud, P. Thuleau, et C. Mazars, « Calcium Sensors as Key
498 Hubs in Plant Responses to Biotic and Abiotic Stresses », *Front. Plant Sci.*, vol. 7, mars 2016, doi:
499 10.3389/fpls.2016.00327.
- 500 [6] W. Tian, C. Wang, Q. Gao, L. Li, et S. Luan, « Calcium spikes, waves and oscillations in plant
501 development and biotic interactions », *Nat. Plants*, vol. 6, n° 7, p. 750-759, juin 2020, doi:
502 10.1038/s41477-020-0667-6.
- 503 [7] G. B. Monshausen, T. N. Bibikova, M. H. Weisenseel, et S. Gilroy, « Ca²⁺ Regulates Reactive
504 Oxygen Species Production and pH during Mechanosensing in *Arabidopsis* Roots », *Plant Cell*,
505 vol. 21, n° 8, p. 2341-2356, août 2009, doi: 10.1105/tpc.109.068395.
- 506 [8] H. Suda *et al.*, « Calcium dynamics during trap closure visualized in transgenic Venus flytrap »,
507 *Nat. Plants*, vol. 6, n° 10, p. 1219-1224, oct. 2020, doi: 10.1038/s41477-020-00773-1.
- 508 [9] A. Voxeur et H. Höfte, « Cell wall integrity signaling in plants: “To grow or not to grow that’s the
509 question” », *Glycobiology*, vol. 26, n° 9, p. 950-960, sept. 2016, doi: 10.1093/glycob/cww029.
- 510 [10] H.-W. Shih, N. D. Miller, C. Dai, E. P. Spalding, et G. B. Monshausen, « The Receptor-like Kinase
511 FERONIA Is Required for Mechanical Signal Transduction in *Arabidopsis* Seedlings », *Current*
512 *Biology*, vol. 24, n° 16, p. 1887-1892, août 2014, doi: 10.1016/j.cub.2014.06.064.

- 513 [11] A.-L. Le Roux, X. Quiroga, N. Walani, M. Arroyo, et P. Roca-Cusachs, « The plasma membrane as a
514 mechanochemical transducer », *Phil. Trans. R. Soc. B*, vol. 374, n° 1779, p. 20180221, août 2019,
515 doi: 10.1098/rstb.2018.0221.
- 516 [12] M. Guichard, S. Thomine, et J.-M. Frachisse, « Mechanotransduction in the spotlight of mechano-
517 sensitive channels », *Current Opinion in Plant Biology*, vol. 68, p. 102252, août 2022, doi:
518 10.1016/j.pbi.2022.102252.
- 519 [13] D. Tran *et al.*, « A mechanosensitive Ca²⁺ channel activity is dependent on the developmental
520 regulator DEK1 », *Nat Commun*, vol. 8, n° 1, p. 1009, déc. 2017, doi: 10.1038/s41467-017-00878-
521 w.
- 522 [14] J.-M. Frachisse, S. Thomine, et J.-M. Allain, « Calcium and plasma membrane force-gated ion
523 channels behind development », *Current Opinion in Plant Biology*, vol. 53, p. 57-64, févr. 2020,
524 doi: 10.1016/j.pbi.2019.10.006.
- 525 [15] R. Dangla, S. C. Kayi, et C. N. Baroud, « Droplet microfluidics driven by gradients of
526 confinement », *Proc. Natl. Acad. Sci. U.S.A.*, vol. 110, n° 3, p. 853-858, janv. 2013, doi:
527 10.1073/pnas.1209186110.
- 528 [16] R. Waadt, M. Krebs, J. Kudla, et K. Schumacher, « Multiparameter imaging of calcium and
529 abscisic acid and high-resolution quantitative calcium measurements using R-GECO1-mTurquoise
530 in Arabidopsis », *New Phytol*, vol. 216, n° 1, p. 303-320, oct. 2017, doi: 10.1111/nph.14706.
- 531 [17] G. Grossmann *et al.*, « The RootChip: An Integrated Microfluidic Chip for Plant Science », *The
532 Plant Cell*, vol. 23, n° 12, p. 4234-4240, déc. 2011, doi: 10.1105/tpc.111.092577.
- 533 [18] M. A. Unger, H.-P. Chou, T. Thorsen, A. Scherer, et S. R. Quake, « Monolithic Microfabricated
534 Valves and Pumps by Multilayer Soft Lithography », *Science*, vol. 288, n° 5463, p. 113-116, avr.
535 2000, doi: 10.1126/science.288.5463.113.
- 536 [19] M. Meier, E. M. Lucchetta, et R. F. Ismagilov, « Chemical stimulation of the Arabidopsis thaliana
537 root using multi-laminar flow on a microfluidic chip », *Lab Chip*, vol. 10, n° 16, p. 2147, 2010, doi:
538 10.1039/c004629a.
- 539 [20] S. A. R. Mousavi *et al.*, « PIEZO ion channel is required for root mechanotransduction in
540 Arabidopsis thaliana », *Proceedings of the National Academy of Sciences*, vol. 118, n° 20, p.
541 e2102188118, mai 2021, doi: 10.1073/pnas.2102188118.
- 542 [21] E. Matthus *et al.*, « DORN1/P2K1 and purino-calcium signalling in plants: making waves with
543 extracellular ATP », *Annals of Botany*, vol. 124, n° 7, p. 1227-1242, déc. 2019, doi:
544 10.1093/aob/mcz135.
- 545 [22] J. Choi *et al.*, « Identification of a plant receptor for extracellular ATP. », *Science (New York, N.Y.)*,
546 vol. 343, n° 6168, p. 290-4, janv. 2014, doi: 10.1126/science.343.6168.290.
- 547 [23] C. T. Nguyen, A. Kurenda, S. Stolz, A. Chételat, et E. E. Farmer, « Identification of cell populations
548 necessary for leaf-to-leaf electrical signaling in a wounded plant », *Proc. Natl. Acad. Sci. U.S.A.*,
549 vol. 115, n° 40, p. 10178-10183, oct. 2018, doi: 10.1073/pnas.1807049115.
- 550 [24] H. Knight, A. J. Trewavas, et M. R. Knight, « Cold calcium signaling in Arabidopsis involves two
551 cellular pools and a change in calcium signature after acclimation. », *Plant Cell*, vol. 8, n° 3, p.
552 489-503, mars 1996, doi: 10.1105/tpc.8.3.489.
- 553 [25] G. J. Allen *et al.*, « A defined range of guard cell calcium oscillation parameters encodes stomatal
554 movements », *Nature*, vol. 411, n° 6841, p. 1053-1057, juin 2001, doi: 10.1038/35082575.
- 555 [26] L. Martin, N. Leblanc-Fournier, J.-L. Julien, B. Mouliat, et C. Coutand, « Acclimation kinetics of
556 physiological and molecular responses of plants to multiple mechanical loadings », *Journal of
557 Experimental Botany*, vol. 61, n° 9, p. 2403-2412, mai 2010, doi: 10.1093/jxb/erq069.
- 558 [27] F. Kramer *et al.*, « Inhibitory glycinergic neurotransmission in the mammalian auditory brainstem
559 upon prolonged stimulation: short-term plasticity and synaptic reliability », *Front. Neural Circuits*,
560 vol. 8, mars 2014, doi: 10.3389/fncir.2014.00014.
- 561 [28] E. Friauf, A. U. Fischer, et M. F. Fuhr, « Synaptic plasticity in the auditory system: a review », *Cell
562 Tissue Res*, vol. 361, n° 1, p. 177-213, juill. 2015, doi: 10.1007/s00441-015-2176-x.

- 563 [29] L. Yue, J. Feng, R. Gaspo, G.-R. Li, Z. Wang, et S. Nattel, « Ionic Remodeling Underlying Action
564 Potential Changes in a Canine Model of Atrial Fibrillation », *Circulation Research*, vol. 81, n° 4, p.
565 512-525, oct. 1997, doi: 10.1161/01.RES.81.4.512.
- 566 [30] S. M. Cain et T. P. Snutch, « Contributions of T-type calcium channel isoforms to neuronal
567 firing », *Channels*, vol. 4, n° 6, p. 475-482, nov. 2010, doi: 10.4161/chan.4.6.14106.
- 568 [31] A. H. Howell *et al.*, « Pavement cells distinguish touch from letting go », *Nat. Plants*, mai 2023,
569 doi: 10.1038/s41477-023-01418-9.
- 570 [32] B. Gardiner, P. Berry, et B. Moulia, « Review: Wind impacts on plant growth, mechanics and
571 damage », *Plant Science*, vol. 245, p. 94-118, avr. 2016, doi: 10.1016/j.plantsci.2016.01.006.
- 572 [33] A. Sampathkumar *et al.*, « Subcellular and supracellular mechanical stress prescribes
573 cytoskeleton behavior in Arabidopsis cotyledon pavement cells », *eLife*, vol. 3, p. e01967, avr.
574 2014, doi: 10.7554/eLife.01967.
- 575 [34] K. R. James, J. R. Moore, D. Slater, et G. A. Dahle, « Tree biomechanics. », *CABI Reviews*, vol.
576 2017, p. 1-11, janv. 2017, doi: 10.1079/PAVSNNR201712038.
- 577 [35] B. Moulia, C. Coutand, et J.-L. Julien, « Mechanosensitive control of plant growth: bearing the
578 load, sensing, transducing, and responding », *Front. Plant Sci.*, vol. 6, févr. 2015, doi:
579 10.3389/fpls.2015.00052.
- 580 [36] T. A. DeFalco, K. W. Bender, et W. A. Snedden, « Breaking the code: Ca²⁺ sensors in plant
581 signalling », *Biochemical Journal*, vol. 425, n° 1, p. 27-40, janv. 2010, doi: 10.1042/BJ20091147.
- 582 [37] F. Resentini *et al.*, « Simultaneous imaging of ER and cytosolic Ca²⁺ dynamics reveals long-
583 distance ER Ca²⁺ waves in plants », *Plant Physiology*, vol. 187, n° 2, p. 603-617, oct. 2021, doi:
584 10.1093/plphys/kiab251.
- 585 [38] S. E. Murthy *et al.*, « OSCA/TMEM63 are an evolutionarily conserved family of mechanically
586 activated ion channels », *eLife*, p. 17, 2018.
- 587 [39] O. Hamant, D. Inoue, D. Bouchez, J. Dumais, et E. Mjolsness, « Are microtubules tension
588 sensors? », *Nat Commun*, vol. 10, n° 1, p. 2360, mai 2019, doi: 10.1038/s41467-019-10207-y.
- 589 [40] A. Fruleux, S. Verger, et A. Boudaoud, « Feeling Stressed or Strained? A Biophysical Model for
590 Cell Wall Mechanosensing in Plants », *Front. Plant Sci.*, vol. 10, p. 757, juin 2019, doi:
591 10.3389/fpls.2019.00757.
- 592 [41] T. Henzler *et al.*, « Diurnal variations in hydraulic conductivity and root pressure can be
593 correlated with the expression of putative aquaporins in the roots of Lotus japonicus », *Planta*,
594 vol. 210, n° 1, p. 50-60, nov. 1999, doi: 10.1007/s004250050653.
- 595 [42] G. L. Richter, G. B. Monshausen, A. Krol, et S. Gilroy, « Mechanical Stimuli Modulate Lateral Root
596 Organogenesis », *Plant Physiol.*, vol. 151, n° 4, p. 1855-1866, déc. 2009, doi:
597 10.1104/pp.109.142448.

598

599

600

601

602

603

604

605

606

607

608 **Supplementary data**

609

610 **Local compression of the root in a microfluidic device triggers a calcium signal**

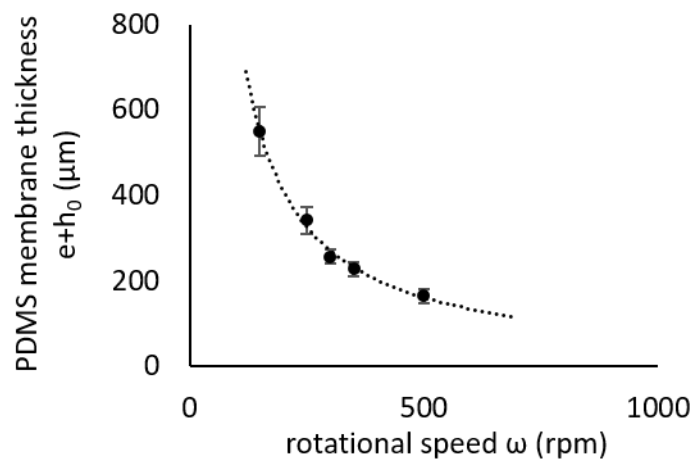
611

612 Vassanti Audemar, Yannick Guerringue, Joni Frederick, Isaty Melogno, Pauline Vinet, Avin
613 Babataheri, Valérie Legué, Sébastien Thomine, Jean-Marie Frachisse

614

615

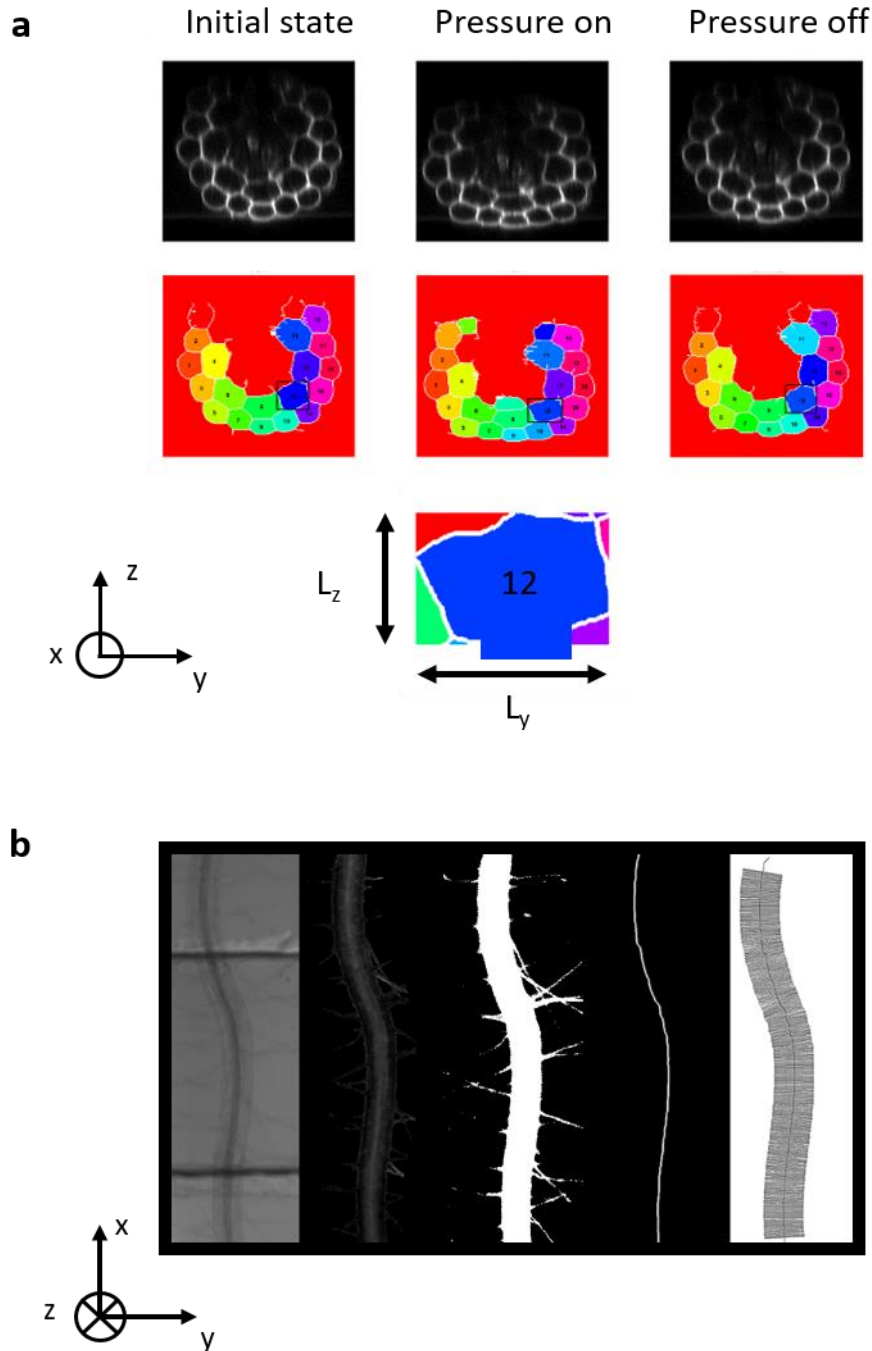
616



617

618 **S-Fig 1:** PDMS membrane thickness variations with ω , the rotational speed during the spin coating
619 process. Circles correspond to experimental data and the dotted line corresponds to the power law
620 fit given by the equation $(e+h_0) = 0.09\omega^{-1,02}$. The fit of the curve with a power law is in agreement
621 with Koschwanez et al. [1] and Zhang et al. [2].

622



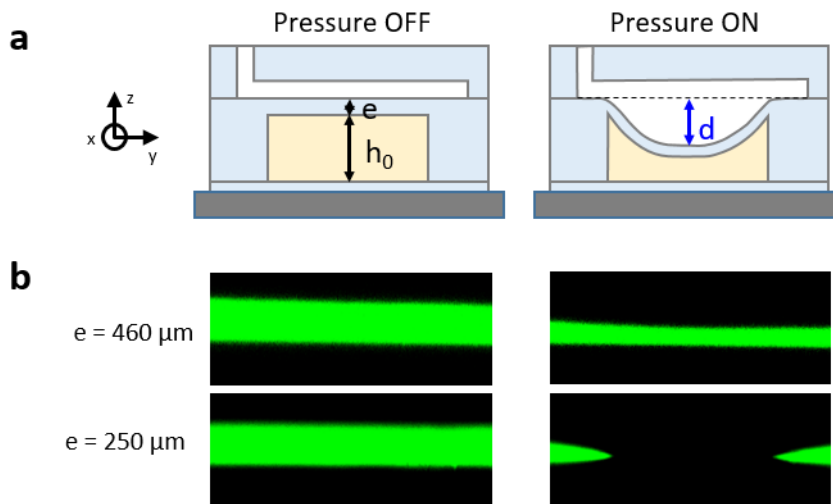
623

624 **S-Fig. 2:** Image analysis procedure: a) Cross-sectional image of the root cells at rest, under a lateral
625 pressure of 900 mbar and after release of the pressure; Top images (black and white), fluorescent
626 images with cell walls colored with propidium iodide (5 $\mu\text{g}/\text{mL}$) and imaged with $\lambda_{\text{exc}} = 488 \text{ nm}$ and
627 $\lambda_{\text{em}} = 551\text{-}651 \text{ nm}$, Middle images (colored), segmented cells separated with white lines, colors have
628 no other purpose than differentiating cells between each other. Cell number 12 is framed by a black
629 bounding box and represented in the bottom line. The maximum height L_z and the maximum width L_y
630 of the cell are indicated. b) Top view image of the root under the valve (from left to right) : bright field
631 image, mTurquoise fluorescent image ($\lambda_{\text{exc}} = 470 \text{ nm}$ and $\lambda_{\text{em}} = 490\text{-}520 \text{ nm}$), binarized image, and
632 skeletonized axis of the root, segments (100 μm length) perpendicular to the root axis and distributed
633 every 50 pixels.

634

635

636



637

638

639 **S-Fig 3:** a) Schematic cross section of the PDMS device showing deformation of the pneumatic valve
640 with and without pressure: e is the thickness of the PDMS membrane separating pressure channel (in
641 white) and the root channel (in yellow), h_0 is the thickness of the root channel without pressure and
642 is equal to $90 \mu\text{m}$, d is the maximum distance between the center of the valve membrane at rest and
643 in its deformed state. b) Cross-sectional view of the microfluidics channels filled with a dilute solution
644 of fluorescein without (left) and with (right) 750 mbar of pressure for two different PDMS membrane
645 thicknesses: $e = 460 \mu\text{m}$ (top image), $e = 250 \mu\text{m}$ (bottom image). Deformability of the PDMS membrane
646 decreases with its thickness.

647

648 Bibliography

649 [1] J. H. Koschwanetz, R. H. Carlson, et D. R. Meldrum, « Thin PDMS Films Using Long Spin Times
650 or Tert-Butyl Alcohol as a Solvent », *PLoS ONE*, vol. 4, n° 2, p. e4572, févr. 2009, doi:
651 10.1371/journal.pone.0004572.

652 [2] W. Y. Zhang, G. S. Ferguson, et S. Tatic-Lucic, « Elastomer-supported cold welding for room
653 temperature wafer-level bonding », in *17th IEEE International Conference on Micro Electro
654 Mechanical Systems. Maastricht MEMS 2004 Technical Digest*, Maastricht, Netherlands, 2004, p.
655 741-744. doi: 10.1109/MEMS.2004.1290691.

656

657

658

659 SUPPLEMENTARY VIDEO 1

660 Deformation of the root stimulated 6 times every 5 min with a pressure of 900 mbar during 1 min.
661 Cross-sectional video of the root with cell walls colored with propidium iodide (5 $\mu\text{g}/\text{mL}$) and imaged
662 with $\lambda_{\text{exc}} = 488 \text{ nm}$ and $\lambda_{\text{em}} = 551\text{-}651 \text{ nm}$. The pressure is applied from the top and the playing speed
663 is accelerated 50 times

664

665 SUPPLEMENTARY VIDEO 2

666 Calcium response of the root to a local pressure of 900 mbar applied during 30 sec (short stimulation).
667 Variations of the normalized ratio RGECO1-mTurquoise fluorescence (λ_{exc} and λ_{em} of RGECO1 and
668 mTurquoise, see Material and Method).The dotted line correspond to the position of the pneumatic
669 valve. The playing speed is accelerated 100 times

670

671 SUPPLEMENTARY VIDEO 3

672 Calcium response of the root to a local pressure of 900 mbar applied during 20 min (long stimulation).
673 Variations of the normalized ratio RGECO1-mTurquoise fluorescence (λ_{exc} and λ_{em} of RGECO1 and
674 mTurquoise, see Material and Method).The dotted line correspond to the position of the pneumatic
675 valve. The playing speed is accelerated 100 times